Spin-label EPR Approaches to Protein Interactions

Son, M. van

3

THE COMPLEX OF CYTOCHROME *C* WITH CYTOCHROME *C* PEROXIDASE STUDIED BY SPIN-LABEL, MULTI-FREQUENCY ELECTRON PARAMAGNETIC RESONANCE

3.1 Introduction

Transient protein-protein complexes are important in biochemical processes, where they often participate in electron transfer. They are designed to provide fast turnover in the crowded cellular environment[1]. The formation of transient complexes has been demonstrated to involve an encounter complex, in which the proteins are loosely bound such that they are free to sample their respective surfaces[2], as well as the more tightly bound, stereo-specific complex, which is capable of electron transfer[3;4]. The process of complex formation is schematically shown in Figure 3.1. Methods are sought to investigate the encounter complex, which is dynamic[5] and could be decisive in making protein encounters specific. The formation of the encounter complex seems to be governed by long-range electrostatic interactions[6;7] and in some cases by hydrophobic interactions[8].

Here we investigate the complex of yeast mitochondrial iso-1-cytochrome *c* (C*c*) with cytochrome *c* peroxidase (CcP), which in yeast is relevant for the removal of hydrogen peroxide. Previously, the interaction of C*c* with CcP has been studied by paramagnetic NMR, revealing that the interaction

of both proteins is best described by an encounter complex that is populated 30% of the time and a stereo-specific complex that is competent for electron transfer and has a 70% occupancy[3-5;8;10;11].

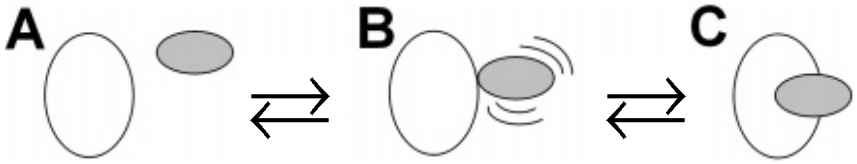

Figure 3.1 A schematic model for the formation of a protein complex. Free partner proteins (A) associate to form an encounter complex (B), in which the proteins are loosely bound such that they are free to sample their respective surfaces. The encounter complex is in equilibrium with a tightly bound stereo-specific complex (C). The figure concerns an edited version of that in reference [9].

We use multi-frequency electron paramagnetic resonance (EPR) at room temperature, where the proteins are in their physiological state, to probe complex formation. The sensitivity of continuous-wave (cw) EPR to the nanosecond motion of a nitroxide spin label covalently attached to the unique cysteine in the A81C mutant of C*c* (C*c*-SL) enables us to probe the local environment of this residue.

Previously, cw-EPR has been used to study the high-affinity protein-protein complex of barnase with barstar[12]. The cw-EPR spectrum of the spin-labelled barnase-barstar complex depends on viscosity, i.e., broad outer peaks of the spin-label signal become more dominant as the viscosity increases[12]. The combination of cw-EPR[13;14] and saturation recovery EPR[13] was applied to the complex of cytochrome bc_1 and spin-labelled cytochrome *c*. For this complex formation, it is shown that altering the NaCl concentration in the

buffer affects the cw-EPR spectra, i.e., the width of the outer peaks of the spin-label signal depends on the ionic strength[13].

We present a systematic approach to analyse a series of EPR spectra obtained at different ratios of the complex partners to determine the dissociation constant. We show how to obtain the spectra of the spin label in the fully-bound state. This is not trivial because the EPR spectra of samples in which both partners are present always contain a fraction in which the spin-labelled partner is not in the complex (free C*c*-SL), even at a large excess of the complex partner (CcP). Since the EPR spectra of free C*c*-SL and bound C*c*-SL have significant overlap and cannot be described by a simple lineshape function (Gaussian or Lorentzian), deconvolution is needed.

By monitoring the complex with a spin label attached to the smaller protein of the complex, the changes in rotation-correlation time upon complex formation are maximized. We show that spectra obtained by conventional X-band (9 GHz) EPR are analysed preferably using principal component analysis (PCA)[15], an approach that is not suited for the high-field, W-band (94 GHz) EPR spectra. To increase spectral resolution even further, EPR at 275 GHz is employed.

We find that the spin label in the A81C-variant of C*c* becomes immobilized upon complex formation. Two fractions with different mobility of the spin label are observed, which could correspond to the encounter and specific complex, respectively. High-field EPR reveals differences between the free and the fully bound state in the anisotropy of the rotation-correlation time of the spin-label motion. Furthermore, the potential of 275 GHz EPR to increase sensitivity to anisotropic motion is addressed.

3.2 Material and methods

Expression and purification of CcP C128A

The expression and purification of CcP C128A was done by Jesika Schilder (Protein Chemistry group at Leiden Institute of Chemistry), who used a procedure previously described[16]. The concentration of CcP was determined with UV-Vis spectroscopy: $\varepsilon_{408nm} = 98\ mM^{-1}\ cm^{-1}$ [17].

Expression and purification of Cc A81C

Chemically competent *E. coli* JM109 cells were freshly transformed with pUC cc A81C plasmid, a pUC18 based plasmid coding for *saccharomyces cerevisiae* C*c* A81C. A single colony was used to inoculate 3 ml of 2×YT medium containing 50 μg/ml ampicillin and 1 mM KNO_3, and incubated at 37 °C, 250 rpm until turbidity was evident (3 – 4 hours). One mL of the pre-culture was used to inoculate 1.7 L of 2×YT medium containing 50 μg/mL ampicillin and 1 mM KNO_3 in a 2 L Erlenmeyer flask and incubated at 37°C, 160 rpm for 24 hours. The cells were harvested by centrifugation at 4 °C, 6400 × *g* for 15 minutes. The pink pellet was re-suspended in a minimum volume of lysis buffer (50 mM Tris-HCl, 1 mM EDTA), flash-frozen in liquid N_2 and stored at –80 ºC. After thawing the cells, 3.8 mg DNAse and a few milligrams of lysozyme and PMSF were added. The suspension was stirred for 30 minutes at 4°C and twice lysed by a pressure cell homogenizer (FPG12800, Stansted Fluid Power Ltd., Harlow, U.K.). Per mL of solution, 326 mg of $(NH_4)_2SO_4$ was added. The solution was stirred at 4°C for 30 minutes. Precipitate was removed by centrifugation at 4°C, 9600 × *g* for 30 min. The supernatant was dialyzed overnight against 5 L of 46 mM NaP_i, pH 6.8. The dialyzed solution was centrifuged at 4°C, 6200 × *g* for 15 minutes and loaded on a CM column (80 mL) equilibrated with 46 mM NaP_i, pH 6.8 at 2 mL/min. The column was

washed with 46 mM NaP_i, pH 6.8, and with 46 mM NaP_i pH 6.8, 70 mM NaCl for two column volumes. C*c* A81C was eluted from the column with 46 mM NaP_i, pH 6.8, 400 mM NaCl, fractions of 2 mL were collected. The fractions showing an absorbance at 550 nm were combined and concentrated to a volume of 2 mL. Dithiothreitol (DTT) was added to the solution to a final concentration of 5 mM. The solution was incubated on ice for 1 hour and run over a Superdex 75 (~ 120 mL) column, pre-equilibrated in 20 mM NaP_i, pH 6.0, 100 mM NaCl, 1 mM DTT, with a flow rate of 1 mL/min, collecting fractions of 1 mL while monitoring the absorption at 280 nm and 550 nm. Fractions with a significant 550 nm signal were combined and concentrated.

This procedure was largely inspired on the procedures described in references [18;19].

Cc A81C spin labelling

C*c* A81C (1 mL of 822 µM) was reduced with 5 mM DTT at 4 °C for 60 minutes. DTT was removed with a 5 mL desalting column (GE Healthcare) equilibrated in 100 mM NaP_i, pH 7.2, 100 mM NaCl (argon bubbled to remove oxygen). Immediately after elution, C*c* A81C was added to a solution of 20 mL 100 mM NaP_i pH 7.2, 100 mM NaCl, 2.2 mM MTSL. This solution was kept at 4 °C for 1 hour while bubbling with argon. The total volume of 23 mL was concentrated to 0.85 mL and kept overnight at 4 °C. Free MTSL was removed by a Superdex 75 gel filtration column (GE Healthcare) equilibrated in 100 mM NaP_i pH 7.2, 100 mM NaCl, The absorption was monitored at 280, 410, and 550 nm and fractions of 1 mL were collected. Fractions with an A_{550}/A_{280} ratio larger than 0.80 were combined and concentrated to 0.7 mL. EPR experiments showed that the spin-labelling efficiency was approximately 93 %. To the protein solution 5 mM $K_3[Fe_3(CN)_6]$ was added. After incubation of 60 minutes, the oxidizing agent was removed by a PD10 column. The protein

solution was concentrated to 0.6 mL. UV-Vis spectroscopy was used to determine the protein concentration of 562 μM (ε_{410nm} = 106.1 mM^{-1} cm^{-1} [19]) and to verify that the protein was oxidized. The protein solution was flash frozen in liquid N_2 and stored at –80 °C.

Important contributions to this procedure were made by Anneloes Blok (Protein Chemistry group at Leiden Institute of Chemistry).

EPR-sample preparation

All EPR samples were prepared in 20 mM NaP_i, 100 mM NaCl, pH 6.0, with protein concentrations based on UV-Vis absorption. For X-band measurements the samples with 100 μM C*c* and varying concentrations of CcP were transferred into 50 μL micropipettes (BLAUBRAND® intraMARK) with an inner/outer diameter (id/od) of 0.80/1.50 mm. For W-band measurements at room temperature the concentration of spin-labelled C*c* was 0.4 mM and samples were placed in suprasil quartz capillaries (Wilmad-Labglass, Buena, NJ, USA) with an id/od of 0.1 mm/0.5 mm. This capillary was put into a suprasil quartz capillary (VitroCom, Mountain Lakes, NJ, USA) with an id/od of 0.60 mm/0.84 mm. At both ends the capillaries were sealed with X-Sealant®. For W-band measurements at 80 K the concentration of spin-labelled C*c* (C*c*-SL) was 0.4 mM and samples were placed in suprasil quartz capillaries (VitroCom, Mountain Lakes, NJ, USA) with an id/od of 0.60 mm/0.84 mm. Both ends were sealed with an epoxy polymer. For the room-temperature measurement at 275 GHz the concentration of C*c*-SL was 3 mM and the sample was measured in a locally made quartz capillary with an id/od of 50 μm/250 μm.

X-band EPR measurements

Measurements at X-band were performed using an ELEXSYS E 680 spectrometer (Bruker BioSpin GmbH, Rheinstetten, Germany) equipped with a rectangular cavity. Spectra were recorded at 0.63 mW microwave power with a modulation amplitude/frequency of 0.2 mT/100 kHz. A 15 mT field sweep of 2048 points was used with a time constant of 10 ms. The total measurement time for a spectrum varied between 35 and 80 minutes. A gentle stream of N_2 was blown through the cavity. A chrome/alumel thermocouple was installed close to the sample to monitor the temperature with a readability of 0.1 K. The temperature during the X-band measurements was 292.6 ± 0.1 K. The buffer in all measurements was 20 mM NaPi, pH 6.0. This buffer had 100 mM NaCl, unless stated otherwise.

EPR measurements at 94 and 275 GHz

For W-band measurements at room temperature and 80 K a locally developed probe head was used combined with a Bruker Elexsys 680 (Bruker BioSpin GmbH, Rheinstetten, Germany) spectrometer. The room-temperature measurement at 275 GHz was done on a locally developed spectrometer [20;21]. Measurements were performed with a modulation amplitude of 0.3 mT (94 GHz, RT), 0.2 mT (94 GHz, 80 K) and 0.6 mT (275 GHz, RT) and a modulation frequency of 10 kHz (94 GHz, RT and 80 K) and 1.7 kHz (275 GHz, RT). The time constant was 82 ms (94 GHz, RT), 41 ms (94 GHz, 80 K) and 1 s (275 GHz, RT). Spectra were recorded with a 30 mT field sweep of 4096 points (94 GHz, RT), a 40 mT field sweep of 4096 points (94 GHz, 80 K), and a 60 mT field sweep of 1051 points (275 GHz, RT). The total measurement time for a recorded spectrum was 120 minutes (94 GHz, RT), 10 minutes (94 GHz, 80 K) and 8 hours (275 GHz, RT). The measurement of C*c*-SL at 275

GHz was done by Peter Gast (Molecular Nano-Optics and Spins group at Leiden Institute of Physics).

Equations to calculate K_D from the fraction of bound complex c

Complex formation and dissociation are described by the equilibrium reaction

$$LP \rightleftarrows L + P, \tag{3.1}$$

where L and P are the complex partners. The dissociation constant K_D is defined as

$$K_D = \frac{[L][P]}{[LP]}, \tag{3.2}$$

where $[L]$ is the concentration of L. Equation 3.2 is rewritten using the total concentrations $[L]_0$ and $[P]_0$:

$$K_D = \frac{(1-c)[L]_0\left([P]_0 - c[L]_0\right)}{c[L]_0}, \tag{3.3}$$

where c is the fraction of L that is bound to P. In the case that c is unknown, equation 3.3 is more conveniently written as

$$c = 0.5[L]_0^{-1}\left\{K_D + [L]_0 + [P]_0 - \sqrt{K_D{}^2 + 2K_D\left([L]_0 + [P]_0\right) + \left([L]_0 - [P]_0\right)^2}\right\}. \tag{3.4}$$

Principal component analysis

Principal component analysis (PCA) is used to decompose a set of spectra into linearly uncorrelated components [22] and was first applied to EPR spectra by Steinbock *et al.*[15]. To apply PCA to the X-band EPR spectra in this work, a script was created in MATLAB (The Mathworks, Natick, MA, USA), which carries out a procedure that is identical to the one given in reference [15]. A set of *n* experimental EPR spectra are integrated to obtain the corresponding absorption spectra. The spectra are then normalized and imported into the script as vectors, $\vec{\mathrm{E}}_i = \vec{\mathrm{E}}_1, \vec{\mathrm{E}}_2, \vec{\mathrm{E}}_3, \ldots, \vec{\mathrm{E}}_n$. Any negative values that are due to noise are set to zero. The vectors, each consisting of *m* points, are stacked to form matrix C consisting of *n* rows and *m* columns. Next, matrix M is obtained by

$$\mathrm{M} = \mathrm{C}^{\mathrm{T}}\mathrm{C}. \tag{3.5}$$

Diagonalization of M is achieved with the MATLAB function `[V,D] = eig(M)`. The diagonal matrix D contains the eigenvalues $\lambda_j = \lambda_\alpha, \lambda_\beta, \lambda_\gamma, \ldots, \lambda_m$, which are associated with the orthonormal eigenvectors $\vec{\mathrm{V}}_j = \vec{\mathrm{V}}_\alpha, \vec{\mathrm{V}}_\beta, \vec{\mathrm{V}}_\gamma, \ldots, \vec{\mathrm{V}}_m$, respectively, contained in V. The eigenvalues are sorted in order of decreasing magnitude so that λ_α has the largest value, λ_β has the second largest value, etc. A non-zero eigenvalue is significant and associated with an eigenvector that is a principal component of the spectrum. Eigenvalues that are zero are associated with eigenvectors that contain only noise. The PCA components can be used in linear combination to reconstruct any of the experimental spectra:

$$\vec{\mathrm{E}}_i = \sum_j c_{ij}\vec{\mathrm{V}}_j \,. \tag{3.6}$$

For the normalized eigenvectors $\vec{V}_j$

$$c_{ij} = \vec{E}_i \cdot \vec{V}_j . \tag{3.7}$$

For a two component system, i.e., only λ_α and λ_β are non-zero, the two coefficients are linearly dependant:

$$c_{i\beta} = ac_{i\alpha} + b \ . \tag{3.8}$$

Along this line, any spectrum $\vec{\Omega}_k$ can be constructed from the eigenvectors $\vec{V}_\alpha$ and $\vec{V}_\beta$ for the points $(c_{k\alpha}, c_{k\beta})$ on the line defined by equation 3.8:

$$\vec{\Omega}_k = c_{k\alpha}\vec{V}_\alpha + c_{k\beta}\vec{V}_\beta . \tag{3.9}$$

The spectra of the pure components correspond to separate points located on the line defined by equation 3.8. Criteria to determine the location of these points have been described in reference [15].

Experimentally measured spectra are decomposed into ‘fraction bound’ and ‘fraction free’ by first locating their position, subsequently referred to as ‘point’, on the line defined by equation 3.9. The difference between the coordinates of the point that defines the position of the experimental spectrum and the point that defines the totally bound spectrum divided by the separation of the fully bound to the fully free spectrum is the ‘fraction of bound spectrum’ present in the experimental spectrum. For the fraction of the free protein the equivalent procedure is used, only then with respect to the point of the free spectrum.

Linear decomposition

The experimental spectrum $\vec{E}$ is composed of the free spectrum $\vec{F}$ and the bound spectrum $\vec{B}$

$$\vec{E} = f\vec{F} + b\vec{B}, \tag{3.10}$$

where f is the fraction of C*c*-SL that is free and b is the fraction bound, i.e., C*c*-SL in complex with CcP. Thus, we can use equation 3.10 to obtain the bound spectrum from the experimental spectrum. For this procedure, the EPR spectra are required to be normalized and superimposed such that the central lines overlap.

Simulation of EPR spectra

The cw-EPR spectra were simulated with EasySpin[23], a software package for MATLAB (The Mathworks, Natick, MA, USA). We manually adjusted the parameters to maximize the similarity between the simulated and the experimental spectrum.

The algorithm *Pepper* was used for the simulation of the W-band spectrum of free C*c*-SL in frozen solution, recorded at 80 K. From this simulation the following spin parameters were obtained: $\vec{\vec{A}}_N$ = [A_{xx} A_{yy} A_{zz}] = [16.0 15.0 104.1] MHz, $\vec{\vec{g}}$ = [g_{xx} g_{yy} g_{zz}] = [2.0088 2.0066 2.0028]. These values were then used for all other simulations.

The algorithm *Garlic* was used for the solution spectra recorded at room temperature. This algorithm allows for the adjustment of the rotation-correlation time, τ_r = [τ_{xx} τ_{yy} τ_{zz}]. We found that the solution spectra are best simulated with two components – one component that represents a fast mobility, the other a slow mobility. We used two restrictions in our approach to

simulate the spectra of free C*c*-SL: i) the τ_r and the ratio of two components were taken equal for the spectra in X-band and W-band; ii) the fast and slow component were given an anisotropic and isotropic rotation, respectively. The same approach was used in the simulation of the X-band and W-band spectra of bound C*c*-SL.

The protein rotation-correlation time

For a globular protein with radius r, the rotation-correlation time is calculated using the Stokes-Einstein relation

$$\tau_r = \frac{4\pi r^3 \eta}{3k_B T}, \tag{3.11}$$

where η is the viscosity of water (1.00 mP·s), k_B the Boltzmann constant, and T is the temperature, in this work: 293 ± 1 K. We used distance measurements in the crystal structure of C*c*:CcP (PDB entry 2PCC[24]) to estimate the radius of C*c* and that of the complex. A hydration radius of 0.24 nm was taken into account.

Calculation with HYDRONMR[25] based on PDB entry 2PCC[24] was used as an alternative route to calculate the isotropic τ_r of C*c* and the complex.

3.3 Results

Figure 3.2 shows a series of X-band EPR spectra of spin-labelled cytochrome *c* (C*c*-SL) measured in the presence of increasing concentrations of cytochrome *c* peroxidase (CcP). The spectrum in Figure 3.2a is that of free C*c*-SL and shows three lines. With CcP added, additional features appear (indicated by arrows in Figure 3.2b to g). With increasing CcP concentration, the intensity of these features increases and the signal intensity of free C*c*-SL decreases. A control experiment with C*c*-SL in a 1:3 ratio with CcP at high salt concentration is shown in yellow in Figure 3.2a. This spectrum is identical to that of free C*c*-SL, indicating that a high ionic strength prevents complex formation.

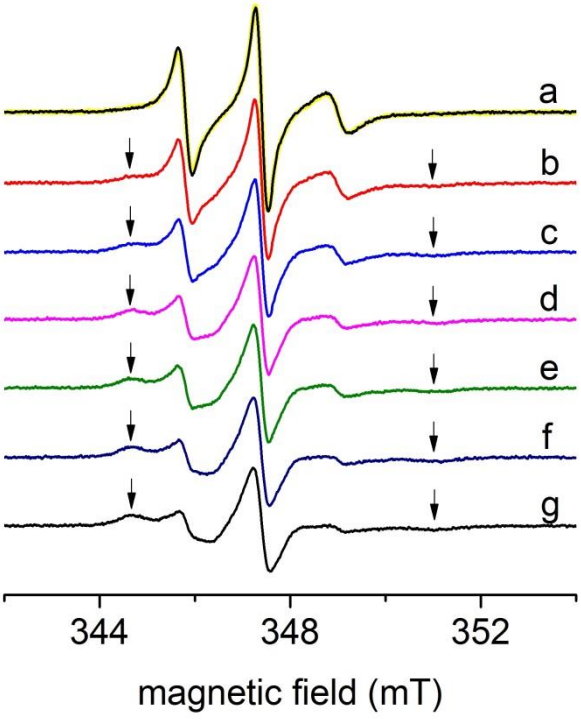

Figure 3.2 The X-band room-temperature EPR spectra of spin-labelled cytochrome *c* (C*c*-SL) with different concentrations of CcP added. (a) 100 µM C*c*-SL without CcP, (b) 100 µM with 50 µM CcP, (c) with 75 µM CcP, (d) with 100 µM CcP, (e) with 133 µM CcP, (f) with 200 µM CcP, and (g) with 400 µM CcP. The arrows indicate lines in spectra (b) to (g) that are not present in spectrum (a). Spectrum (a) is overlaid with the spectrum of 135 µM C*c*-SL, 388 µM CcP with 556 mM NaCl (in yellow).

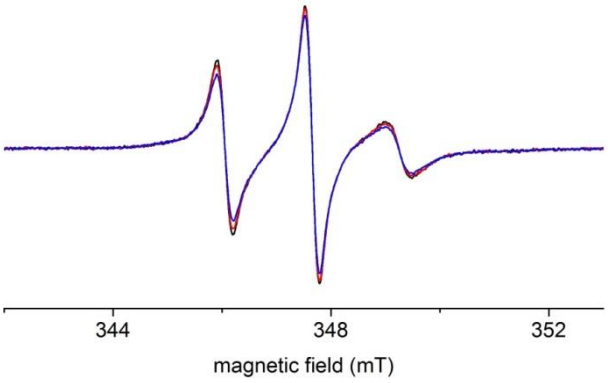

Figure 3.3 The X-band room-temperature EPR spectra of C*c*-SL with bovine serum albumin (BSA). In black: 161 µM C*c*-SL; in red: 161 µM C*c*-SL with 161 µM BSA; in blue: 161 µM C*c*-SL with 430 µM BSA.

In Figure 3.3, the X-band EPR spectra are shown of C*c*-SL measured with bovine serum albumin (BSA), a protein that should not bind Cc specifically and is therefore suitable as a control. The figure shows the spectrum of C*c*-SL alone, in 1:1 and 1:2.7 mixture with BSA. The three spectra are not identical; with increasing concentration of BSA a subtle line broadening is detected compared to the spectrum of C*c*-SL alone, suggesting a very weak, non-specific interaction between the proteins. Nonetheless, the spectral changes detected in the spectra of C*c*-SL with BSA are much smaller than in spectra of samples in which CcP is added (Figure 3.2).

Figure 3.4 shows the W-band EPR spectra of C*c*-SL measured with different concentrations of CcP. With CcP added, features are visible (indicated by arrows in Figure 3.4b to d) that correspond to a signal with broader lines than the free C*c*-SL (Figure 3.4a), particularly in the high-field region. In Figure 3.4a and b the asterisks indicate a background signal that was also encountered when an empty quartz capillary is measured (data not shown). The asterisks in Figure 3.4c indicate the sharp lines that likely originate from a manganese impurity.

The frozen-solution spectra of C*c*-SL (Figure 3.4e) and C*c*-SL:CcP 1:1 (Figure 3.4f) have singularities at identical field positions revealing that the $\vec{\vec{g}}$

and $\vec{\vec{A}}_N$ parameters of free C*c*-SL and the bound form do not differ significantly in the frozen state. Therefore, $\vec{\vec{g}}$ and $\vec{\vec{A}}_N$ parameters for the simulation of the solution spectra were derived from the simulation of the spectrum in Figure 3.4e.

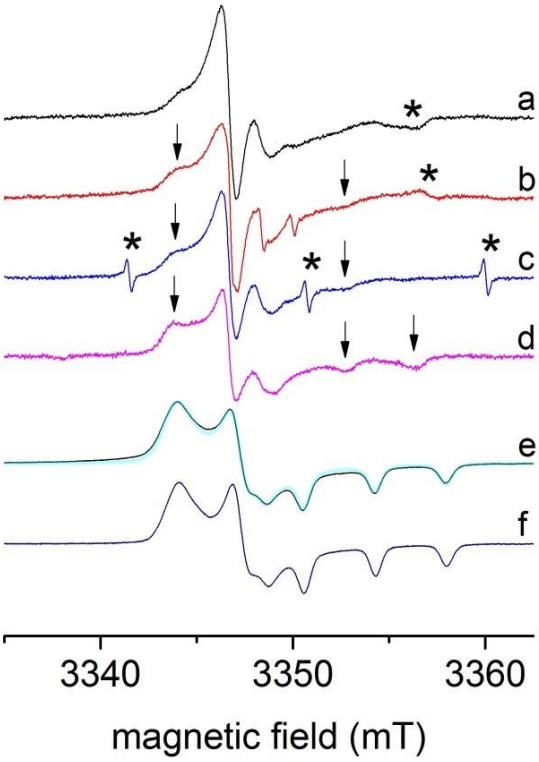

Figure 3.4 The W-band EPR spectra of C*c*-SL with different concentrations of CcP at room temperature (RT) and at 80 K. 400 µM C*c*-SL (a) without CcP (RT), (b) with 100 µM CcP (RT), (c) with 200 µM CcP (RT), (d) 414 µM C*c*-SL with 400 µM CcP (RT), (e) 482 µM C*c*-SL without CcP (80 K), and (f) 371 µM C*c*-SL with 373 µM CcP (80 K). In the room-temperature spectra, the arrows indicate lines that are more pronounced than in the spectrum shown in (a). The asterisk in (a) and (b) indicates a background signal. The asterisks in (c) indicate sharp lines that likely originate from a manganese impurity. The spectrum of free C*c*-SL recorded at 80 K, shown in (e), was used for simulation (in cyan) to obtain the tensors $\vec{\vec{g}}$ and $\vec{\vec{A}}_N$ given in Material and Methods.

Figure 3.5 displays the room-temperature EPR spectrum of free C*c*-SL recorded at 275 GHz. A sharp line, indicated by an asterisk, is attributed to a manganese impurity. The spectrum spreads over 50 mT, whereas the W-band spectrum has a spread of less than 20 mT, showing the higher resolving power of 275 GHz EPR. The 275 GHz spectrum has features at the field values marked g_{xx}, g_{yy} and a broad, low intensity band around the field value marked g_{zz}.

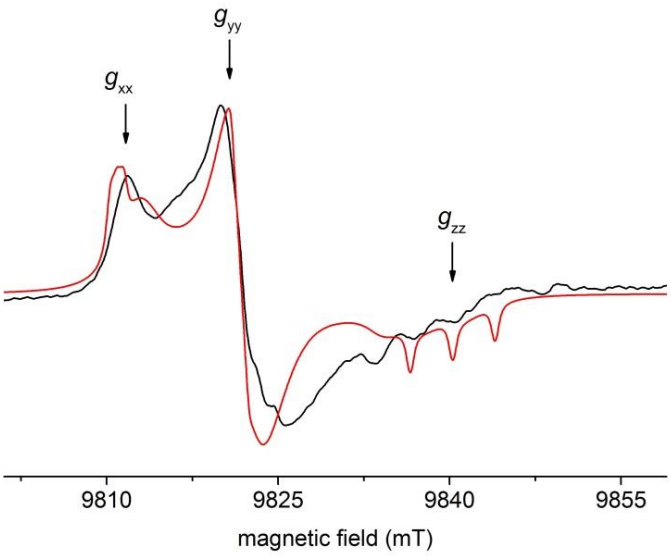

Figure 3.5 The room-temperature EPR spectrum of free C*c*-SL recorded at 275 GHz. The experimental spectrum (shown in black) contains an underlying powder spectrum, which is revealed by the pronounced feature at g_{xx}. A mix of a solution spectrum (70%) and a powder spectrum (30%) was used to obtain the simulation (shown in red). We used the g and A_N tensor values as given in Material and methods. Furthermore, we used the rotation-correlation times and fraction ratios of the free C*c*-SL (see Table 3.1) and a combination of a Gaussian and Lorentzian lineshape (0.2 mT and 0.4 mT linewidth, respectively). The powder spectrum was obtained with the algorithm *Pepper*.

The PCA analysis of the X-band EPR spectra from Figure 3.2 yielded two eigenvalues that were non-zero: λ_α = 1.875 and λ_β = 0.019. Consequently, the

EPR spectra derive from a two-component system. Figure 3.6 shows the result of the PCA analysis on the X-band spectra. The values for $c_{i\alpha}$ and $c_{i\beta}$, obtained from equation 3.7, are plotted in Figure 3.6a. A linear fit through the points yields the relation

$$c_{i\beta} = 1.55 - 3.00\, c_{i\alpha}\,. \tag{3.12}$$

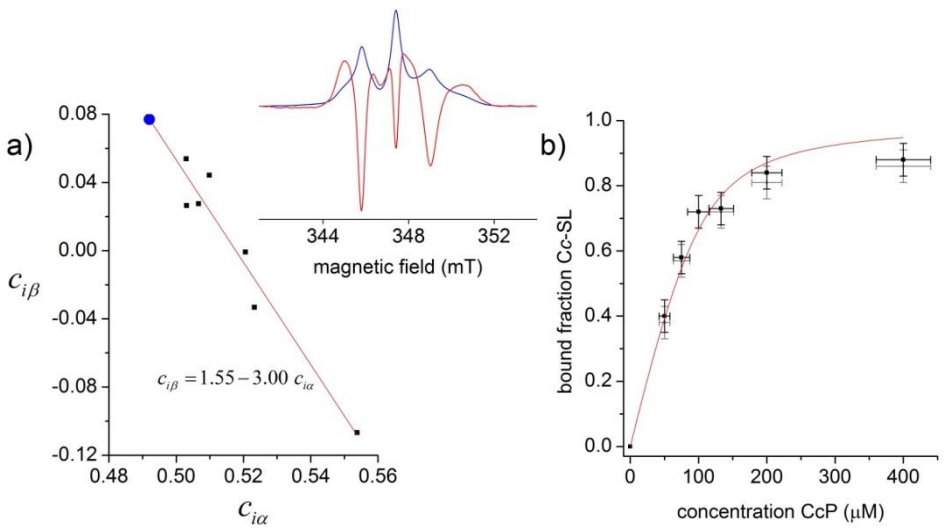

Figure 3.6 Result of the PCA analysis of the X-band spectra of C*c*-SL:CcP (see Figure 3.2). a) Black dots: $(c_{i\alpha}, c_{i\beta})$ points of the experimental spectra. The trend line (in red) is obtained by a linear fit through the seven points. The blue dot marks the position of the fully bound spectrum, point $(c_{i\alpha}, c_{i\beta})$ = (0.491, 0.077). Inset: eigenvectors $\bar{V}_\alpha$ (in blue) and $\bar{V}_\beta$ (in red). b) The bound fractions of C*c*-SL versus the concentration of CcP in the seven X-band EPR measurements obtained by PCA (in black) and obtained by linear decomposition (in grey). The horizontal error bars represent the uncertainty in the CcP concentrations due to multiple dilution steps in the preparation of the EPR samples. The vertical error bars represent the uncertainty in determining the fraction of bound C*c*-SL and is mainly caused by the noise level in the EPR spectra. The dissociation constant, $K_D = 17 \pm 3$ μM, was determined by a fit (red line) with equation 3.4.

The eigenvectors $\vec{V}_\alpha$ and $\vec{V}_\beta$ that resulted from the PCA analysis are shown as an inset in Figure 3.6a. With these eigenvectors and equations 3.9 and 3.12, several spectra were inspected in the range $0.480 \le c_{i\alpha} \le 0.500$ to determine the bound spectrum. The spectrum selected as the most bound spectrum is shown in Figure 3.7c. This point is $(c_{i\alpha}, c_{i\beta})$ = (0.491, 0.077) and is shown in Figure 3.6a as a blue dot. From the PCA analysis, the fraction of bound C*c*-SL (b) for each measurement was determined by the following equation:

$$b = \frac{c_{i\beta}(\text{measurement}) - c_{i\beta}(\text{free})}{c_{i\beta}(\text{bound}) - c_{i\beta}(\text{free})}. \qquad (3.13)$$

To determine K_D, in Figure 3.6b the fraction of bound C*c*-SL derived from the PCA analysis is plotted versus the concentration of CcP in the seven measurements (see Figure 3.2). The dissociation constant that best fits this data (equation 3.4) is K_D = 17 ± 3 μM.

Linear decomposition resulted in a K_D that is identical within the error margins. The W-band EPR spectra showed four principal components in PCA, rather than the two components expected from the results of the X-band EPR spectra. We attribute the additional components to spurious signals and baseline instabilities, which are more pronounced in the W-band than in the X-band EPR spectra, and therefore abandoned PCA on the W-band EPR spectra.

Analysis by linear decomposition works better. To extract the fully bound spectrum, a fraction of the free spectrum of C*c*-SL (Figure 3.4a) was subtracted from the spectrum in Figure 3.4d. The amount of free spectrum was varied in the range of 10% to 50% and the value of 20% was selected by visual inspection resulting in the spectrum shown in Figure 3.7d.

Rotation-correlation times of the spin label were determined by simulations of the spectra of free C*c*-SL and of C*c*-SL fully bound to CcP (C*c*-SL:CcP, Figure 3.7). To satisfactorily simulate the X-band and the W-band spectra, two components were used, one of which had a rhombic rotation tensor. Models including an ordering potential[26] were not tried. In free C*c*-SL, a majority fraction (60%) of the spin label rotates with a τ_r that is anisotropic and overall smaller than the τ_r of the protein (Table 3.1). The second fraction is isotropic and has a τ_r close to that of the protein. The simulation parameters are also compatible with the 275 GHz EPR spectrum of free C*c*-SL (Figure 3.5).

Table 3.1 The parameters used for the simulation of cw-EPR spectra of spin-labelled cytochrome *c* alone (free) and in complex with cytochrome *c* peroxidase (bound).

	fast component [a]					slow component [a]		protein/complex	
state of C*c*-SL	τ_{xx} (ns)	τ_{yy} (ns)	τ_{zz} (ns)	isotropic τ_r(ns)	fraction	isotropic τ_r(ns)	fraction	isotropic τ_r (ns)	
free	2	0.7	3	1.3	60%	5	40%	5.6 [b]	7.3 [c]
bound	8	1.5	8	3.3	20%	8	80%	18.5 [b]	29 [c]

[a] The spectral lines were described with a Gaussian (g) and/or Lorentzian (l) lineshape. The linewidths used were: X-band free: 0.03 mT (g), 0.04 mT (l) / W-band free: 0.3 mT (l) / X-band bound: 0.07 mT (g)/ W-band bound: 0.1 mT (l).

[b] The values were calculated with equation 3.11.

[c] The values were calculated with HYDRONMR[25] (see Material and Methods).

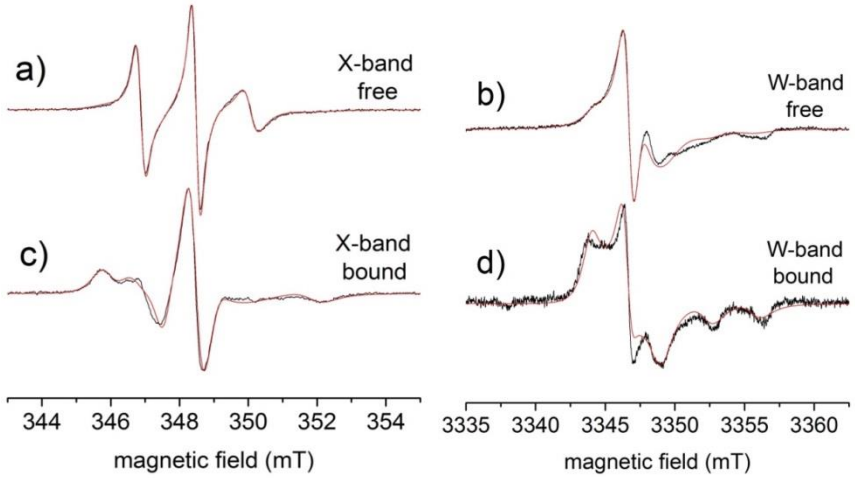

Figure 3.7 The free and bound spectra of C*c*-SL in solution at X-band and W-band. The experimental and simulated data are shown in black and red, respectively. The experimental data in a) and b) are spectra directly obtained from measurement. The experimental data in c) was obtained via PCA (see Material and methods) applied to the spectra shown in Figure 3.2. The experimental data in d) was obtained via linear decomposition (see Material and methods) of the spectra shown in Figures 3.4a and d. The simulations were obtained with the parameters listed in Table 3.1. Note: for the spectra in a) and c) an up-field shift of 1.1 mT was applied compared to the spectra in Figure 3.2.

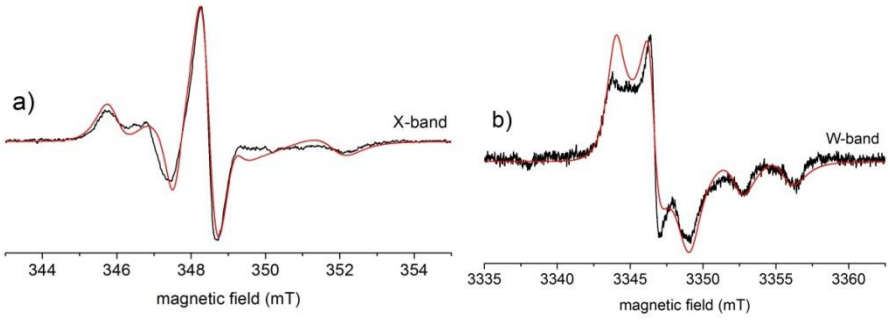

Figure 3.8 Simulations of the fully bound spectrum showing the effect of the fast component on the spectra. Simulations (red) of X-band (a) and W-band (b) spectrum without the fast component, i.e., using only an isotropic rotation-correlation time of 8 ns. The experimental spectra are identical to the spectra in Figures 3.7c and d.

In the fully-bound state, the rotation is slower than for free C*c*-SL. The larger fraction (80%) has an isotropic rotation with a τ_r of 8 ns, and the smaller fraction has an anisotropic rotation, with an average τ_r that is about twice as long as that of the fast fraction in the free C*c*-SL. The anisotropic rotation has the smallest component along the *y*-axis of the nitroxide in the simulations of both spectra. Simulation parameters may not be unique, and, in particular, several solutions for the anisotropy of the rotation were found, which agree with the data. Figure 3.8 shows the same experimental spectra as in Figures 3.7c and d and simulations of the spectra, which were obtained with an isotropic τ_r of 8 ns, i.e., in which for the smaller, fast component in Table 3.1 is omitted. The simulations in Figures 3.8a and b agree less with the experimental spectra than in Figures 3.7c and d, which illustrates that the smaller fraction is essential for a satisfactory interpretation of the bound spectra.

The parameter set given in Table 3.1 fits best to the X- and the W-band spectra simultaneously. We have not systematically investigated whether there are correlations between different simulation parameters, e.g. the contribution of components and τ_r, such as described earlier[26]. The overall rotation of the free C*c*-SL is faster than for C*c*-SL in the complex with CcP.

3.4 Discussion

We show an approach to locally map the environment at the interface of a transient complex. To do so, a set of EPR spectra of samples with different ratios of complex-binding partners has been analysed. The fully overlapping spectra were disentangled to obtain K_D and the spectra of the free and fully bound states. We employ the sensitivity of multi-frequency EPR to nanosecond motion of a spin label and determine the change in the rotation-correlation time of the spin label as the complex is formed.

Systematic changes in motion of the spin label attached to C*c* (C*c*-SL) occur, when C*c*-SL is in the presence of the complex-binding partner (CcP), Figures 3.2 and 3.4. At salt concentrations known to disrupt the complex, these changes disappear (Figure 3.2a). The spectral changes, therefore, are due to complex formation and not caused by an increase of the solution viscosity due to the presence of the complex partner. The small spectral changes observed when adding BSA, a protein we used as a negative control (Figure 3.3), must be due to unspecific binding. Having thus established that the spectra monitor complex formation, we proceed to further characterize the spectra.

To map the change in spin-label motion in the free and fully bound state of C*c*-SL, spectral analysis is performed. Particularly, the spectrum of C*c*-SL in complex with CcP needs attention, because mixtures of C*c*-SL and CcP always contain a fraction of free C*c*-SL, even at a large excess of CcP. A contribution of free C*c*-SL in the order of 5% remains and since the spectrum of free C*c*-SL has narrower lines than that of C*c*-SL in complex with CcP (see below), the free C*c*-SL contribution disturbs the lineshape. We used PCA and linear decomposition to determine the EPR spectrum of bound C*c*-SL and the fraction by which this spectrum contributes to the experimental spectra of mixtures of C*c*-SL with different ratios of CcP. The fraction of bound C*c*-SL serves to determine the K_D value (see Results). The K_D thus obtained (17 ± 3

μM) agrees well with the results of recent NMR experiments: K_D = 19 ± 4 μM[27], which were performed on the protein construct A81C linked with a diamagnetic variant of the spin label, showing that EPR and NMR monitor the same state of the complex. Spin-label dynamics of free C*c*-SL and fully bound C*c*-SL differ considerably. The free C*c*-SL contains a large fraction of a mobile component. Since the rotation-correlation time is smaller than that of the protein, local mobility, i.e., rotation about the single bonds linking the spin label to the protein backbone is dominant in that fraction. The local motion is frozen out in the second fraction, and the nitroxide must be locked to the protein. The spin label is either completely immobilized at the protein surface, or, if it has residual motion, the correlation time of this motion must be larger than 5.6 ns, the τ_r of the protein.

When C*c*-SL is in complex with CcP, the local mobility of the spin label is reduced, leading to larger τ_r values and a smaller fraction of the mobile form (20% compared to 60% in the free form). To demonstrate the validity of the interpretation of two fractions, in Fig. 3.8 we compare the fully bound spectrum with simulations in which the mobile fraction is omitted. Notably, the simulation of the X-band spectrum is still acceptable, but the W-band spectrum is not compatible with that interpretation. This demonstrates that by high-field EPR, previously inaccessible detail of complex formation can be determined. In Fig. 3.5, we show that this limit can be pushed even further. The spectrum at 275 GHz, measured on the free C*c*-SL at 3 mM concentration shows that a sufficiently high signal-to-noise ratio can be achieved to perform lineshape analysis in the future.

According to NMR studies, in the wild-type C*c*:CcP about 30% of the complex is in the dynamic, encounter state, while the rest is in the productive, specific complex, suitable for electron transfer[10]. One could speculate that the

20% fraction observed by EPR is due to proteins in the encounter complex, whereas the slower fraction is the protein in the stereo-specific complex. Under these assumptions, the spin label in the stereo-specific complex would be pinned to the interaction surface of both proteins. Residual mobility could still be present, because the τ_r of this fraction is smaller than the τ_r calculated for the protein complex. Consequently, the more mobile fraction would be due to the encounter complex and the spin-label mobility would reflect the dynamics and local structure of the encounter complex. In our simulations, the additional mobility component manifests itself in a faster rotation about the spin-label g_{yy}-axis (see Figure 1.2), suggesting that in the encounter complex the spin label is more free to rotate about this axis. Additional simulations are needed to prove this anisotropic rotation model, simulations that would be aided by 275 GHz experiments to be performed in the future.

Immobilization upon complex formation has been found before for the complex of C*c* with cytochrome bc_1 by Sarewicz et al.[28]. Novel in the present study is the possibility to discriminate between two fractions in the EPR spectra, potentially related to the encounter and the stereospecific complex (fast and mobile fractions).

References

[1] M. Ubbink, The courtship of proteins: Understanding the encounter complex. Febs Letters **583** (2009) 1060-1066.

[2] Y.C. Kim, C. Tang, G.M. Clore, G. Hummer, Replica exchange simulations of transient encounter complexes in protein-protein association. Proceedings of the National Academy of Sciences of the United States of America **105** (2008) 12855-12860.

[3] A.N. Volkov, J.A.R. Worrall, E. Holtzmann, M. Ubbink, Solution structure and dynamics of the complex between cytochrome c and cytochrome c peroxidase determined by paramagnetic NMR. Proceedings of the National Academy of Sciences of the United States of America **103** (2006) 18945-18950.

[4] M. Prudencio, M. Ubbink, Transient complexes of redox proteins: structural and dynamic details from NMR studies. Journal of Molecular Recognition **17** (2004) 524-539.

[5] J. Schilder, M. Ubbink, Formation of transient protein complexes. Current Opinion in Structural Biology **23** (2013) 911-918.

[6] T. Selzer, G. Schreiber, New insights into the mechanism of protein-protein association. Proteins-Structure Function and Genetics **45** (2001) 190-198.

[7] F.B. Sheinerman, R. Norel, B. Honig, Electrostatic aspects of protein-protein interactions. Current Opinion in Structural Biology **10** (2000) 153-159.

[8] I. Diaz-Moreno, A. Diaz-Quintana, M.A. De la Rosa, M. Ubbink, Structure of the complex between plastocyanin and cytochrome f from the cyanobacterium Nostoc sp PCC 7119 as determined by paramagnetic NMR - The balance between electrostatic and hydrophobic interactions within the transient complex determines the relative orientation of the two proteins. Journal of Biological Chemistry **280** (2005) 18908-18915.

[9] R. Hulsker, M.V. Baranova, G.S. Bullerjahn, M. Ubbink, Dynamics in the transient complex of plastocyanin-cytochrome f from Prochlorothrix hollandica. Journal of the American Chemical Society **130** (2008) 1985-1991.

[10] Q. Bashir, A.N. Volkov, G.M. Ullmann, M. Ubbink, Visualization of the Encounter Ensemble of the Transient Electron Transfer Complex of Cytochrome c and Cytochrome c Peroxidase. Journal of the American Chemical Society **132** (2010) 241-247.

[11] A.N. Volkov, Transient Complexes of Heam Proteins, dissertation, Leiden University (2007).

[12] V.P. Timofeev, V.V. Novikov, Y.V. Tkachev, T.G. Balandin, A.A. Makarov, S.M. Deyev, Spin label method reveals barnase-barstar interaction: A temperature and viscosity dependence approach. Journal of Biomolecular Structure & Dynamics **25** (2008) 525-534.

[13] M. Sarewicz, A. Borek, F. Daldal, W. Froncisz, A. Osyczka, Demonstration of short-lived complexes of cytochrome c with cytochrome bc(1) by EPR spectroscopy - Implications for the mechanism of interprotein electron transfer. Journal of Biological Chemistry **283** (2008) 24826-24836.

[14] M. Sarewicz, S. Szytula, M. Dutka, A. Osyczka, W. Froncisz, Estimation of binding parameters for the protein-protein interaction using a site-directed spin labeling and EPR spectroscopy. European Biophysics Journal with Biophysics Letters **37** (2008) 483-493.

[15] O. Steinbock, B. Neumann, B. Cage, J. Saltiel, S.C. Muller, N.S. Dalal, A demonstration of principal component analysis for EPR spectroscopy: Identifying pure component spectra from complex spectra. Analytical Chemistry **69** (1997) 3708-3713.

[16] J. Schilder, F. Lohr, H. Schwalbe, M. Ubbink, The cytochrome c peroxidase and cytochrome c encounter complex: The other side of the story. Febs Letters **588** (2014) 1873-1878.

[17] J.A.R. Worrall, U. Kolczak, G.W. Canters, M. Ubbink, Interaction of yeast iso-1-cytochrome c with cytochrome c peroxidase investigated by [N-15,H-1] heteronuclear NMR spectroscopy. Biochemistry **40** (2001) 7069-7076.

[18] W.B.R. Pollock, F.I. Rosell, M.B. Twitchett, M.E. Dumont, A.G. Mauk, Bacterial expression of a mitochondrial cytochrome c. Trimethylation of Lys72 in yeast iso-1-cytochrome c and the alkaline conformational transition. Biochemistry **37** (1998) 6124-6131.

[19] A.S. Morar, D. Kakouras, G.B. Young, J. Boyd, G.J. Pielak, Expression of N-15-labeled eukaryotic cytochrome c in Escherichia coli. Journal of Biological Inorganic Chemistry **4** (1999) 220-222.

[20] H. Blok, J.A.J.M. Disselhorst, S.B. Orlinskii, J. Schmidt, A continuous-wave and pulsed electron spin resonance spectrometer operating at 275 GHz. Journal of Magnetic Resonance **166** (2004) 92-99.

[21] G. Mathies, H. Blok, J.A.J.M. Disselhorst, P. Gast, H. van der Meer, D.M. Miedema, R.M. Almeida, J.J.G. Moura, W.R. Hagen, E.J.J. Groenen, Continuous-wave EPR at 275 GHz: Application to high-spin Fe3+ systems. Journal of Magnetic Resonance **210** (2011) 126-132.

[22] K.R. Beebe, B.R. Kowalski, An Introduction to Multivariate Calibration and Analysis. Analytical Chemistry **59** (1987) 1007 A-1017 A.

[23] S. Stoll, A. Schweiger, EasySpin, a comprehensive software package for spectral simulation and analysis in EPR. Journal of Magnetic Resonance **178** (2006) 42-55.

[24] H. Pelletier, J. Kraut, Crystal-Structure of A Complex Between Electron-Transfer Partners, Cytochrome-C Peroxidase and Cytochrome-C. Science **258** (1992) 1748-1755.

[25] J.G. de la Torre, M.L. Huertas, B. Carrasco, HYDRONMR: Prediction of NMR relaxation of globular proteins from atomic-level structures and hydrodynamic calculations. Journal of Magnetic Resonance **147** (2000) 138-146.

[26] D.E. Budil, S. Lee, S. Saxena, J.H. Freed, Nonlinear-least-squares analysis of slow-motion EPR spectra in one and two dimensions using a modified Levenberg-Marquardt algorithm. Journal of Magnetic Resonance Series A **120** (1996) 155-189.

[27] J. Schilder, *et al*., *work to be published*.

[28] M. Sarewicz, A. Borek, F. Daldal, W. Froncisz, A. Osyczka, Estimation of the lifetime of the complex between cytochrome c and cytochrome bc(1) using electron paramagnetic resonance. Biochimica et Biophysica Acta-Bioenergetics **1777** (2008) S103.